Original Article

MOLECULAR METABOLISM

RIPK3 promotes islet amyloid-induced β-cell loss and glucose intolerance in a humanized mouse model of type 2 diabetes

Noyonika Mukherjee [1], Christopher J. Contreras [2], Li Lin [3], Kaitlyn A. Colglazier [3], Egan G. Mather [3], Michael A. Kalwat [3], Nathalie Esser [4], Steven E. Kahn [4], Andrew T. Templin [1,2,3,5,*]

ABSTRACT

Objective: Aggregation of human islet amyloid polypeptide (hIAPP), a β-cell secretory product, leads to islet amyloid deposition, islet inflammation and β-cell loss in type 2 diabetes (T2D), but the mechanisms that underlie this process are incompletely understood. Receptor interacting protein kinase 3 (RIPK3) is a pro-death signaling molecule that has recently been implicated in amyloid-associated brain pathology and β-cell cytotoxicity. Here, we evaluated the role of RIPK3 in amyloid-induced β-cell loss using a humanized mouse model of T2D that expresses hIAPP and is prone to islet amyloid formation.

Methods: We quantified amyloid deposition, cell death and caspase 3/7 activity in islets isolated from WT, Ripk3$^{-/-}$, hIAPP and hIAPP; Ripk3$^{-/-}$ mice in real time, and evaluated hIAPP-stimulated inflammation in WT and Ripk3$^{-/-}$ bone marrow derived macrophages (BMDMs) *in vitro*. We also characterized the role of RIPK3 in glucose stimulated insulin secretion (GSIS) *in vitro* and *in vivo*. Finally, we examined the role of RIPK3 in high fat diet (HFD)-induced islet amyloid deposition, β-cell loss and glucose homeostasis *in vivo*.

Results: We found that amyloid-prone hIAPP mouse islets exhibited increased cell death and caspase 3/7 activity compared to amyloid-free WT islets *in vitro*, and this was associated with increased RIPK3 expression. hIAPP; Ripk3$^{-/-}$ islets were protected from amyloid-induced cell death compared to hIAPP islets *in vitro*, although amyloid deposition and caspase 3/7 activity were not different between genotypes. We observed that macrophages are a source of *Ripk3* expression in isolated islets, and that Ripk3$^{-/-}$ BMDMs were protected from hIAPP-stimulated inflammatory gene expression (*Tnf*, *Il1b*, *Nos2*). Following 52 weeks of HFD feeding, islet amyloid-prone hIAPP mice exhibited impaired glucose tolerance and decreased β-cell area compared to WT mice *in vivo*, whereas hIAPP; Ripk3$^{-/-}$ mice were protected from these impairments.

Conclusions: In conclusion, loss of RIPK3 protects from amyloid-induced inflammation and islet cell death *in vitro* and amyloid-induced β-cell loss and glucose intolerance *in vivo*. We propose that therapies targeting RIPK3 may reduce islet inflammation and β-cell loss and improve glucose homeostasis in the pathogenesis of T2D.

Keywords RIPK3; Islet amyloid; β-cell cytotoxicity; Diabetes

1. INTRODUCTION

Type 2 diabetes (T2D) is a global epidemic characterized by insulin resistance, loss of functional β-cell mass and hyperglycemia [1,2]. Islet amyloid deposits are present in the majority of individuals with T2D, where they are associated with islet inflammation, decreased β-cell mass and increased β-cell death [3–6]. Islet amyloidosis occurs via aggregation of human islet amyloid polypeptide (hIAPP), a β-cell secretory product that is co-secreted with insulin [7,8]. In contrast to hIAPP, rodent IAPP (rIAPP) does not aggregate to form amyloid [8,9], so mouse models with β-cell expression of hIAPP have been developed to model islet amyloidosis in T2D [10,11]. Several studies have found that oligomeric forms of hIAPP directly elicit β-cell cytotoxicity, either by disrupting cell membranes [9,12–14] or by inducing receptor-mediated cell death signaling [15,16]. In addition, islet amyloid formation is thought to mediate β-cell loss by eliciting cytokine (*Il1b, Tnf, Il6*) and chemokine (*Ccl2, Cxcl1*) production from islet macrophages [5,17–19]. Although prior research has established that amyloid formation is an important mediator of islet inflammation and β-cell cytotoxicity in T2D, the molecular mechanisms that underlie this process remain incompletely understood.

Recent studies of amyloid-induced cytotoxicity in Alzheimer's disease (AD) identified receptor interacting protein kinase 3 (RIPK3) as a mediator of neuronal cell loss in this disease [20–22]. RIPK3 is a multifunctional protein that regulates inflammation and cell death signaling in diverse cell types including neurons [20], hepatocytes [23],

[1]Department of Biochemistry & Molecular Biology, Indiana University School of Medicine, Indianapolis, IN, USA [2]Division of Endocrinology, Department of Medicine, Roudebush VA Medical Center and Indiana University School of Medicine, Indianapolis, IN, USA [3]Lilly Diabetes Center of Excellence, Indiana Biosciences Research Institute, Indianapolis, IN, USA [4]Division of Metabolism, Endocrinology and Nutrition, Department of Medicine, VA Puget Sound Health Care System and the University of Washington, Seattle, WA, USA [5]Center for Diabetes and Metabolic Diseases, Indiana University School of Medicine, Indianapolis, IN, USA

*Corresponding author. 1210 Waterway Blvd., Ste. 2000, Indianapolis, IN, 46202, USA. E-mail: templin@iu.edu (A.T. Templin).

Received November 6, 2023 • Revision received December 29, 2023 • Accepted January 9, 2024 • Available online 11 January 2024

https://doi.org/10.1016/j.molmet.2024.101877

immune cells [24] and β cells [25,26]. RIPK3 promotes inflammation in part by mediating IL-1β, IL-6, CXCL1 and CCL2 synthesis [24,27,28], and it also participates in apoptotic and necroptotic cell death signaling via effects on caspase activation [29,30] and mixed lineage kinase domain like pseudokinase (MLKL) phosphorylation, respectively [23,31]. Yang and colleagues previously showed that RIPK3 promotes islet inflammation following ER stress [25], and we recently reported that RIPK3 contributes to TNFα-induced β-cell death [26]. However, the role of RIPK3 in islet amyloid-induced β-cell cytotoxicity and hyperglycemia has not been evaluated previously.

We hypothesized that RIPK3 mediates amyloid-induced β-cell loss and hyperglycemia in T2D. To test this hypothesis, we used a well characterized humanized mouse model of T2D with β-cell specific expression of hIAPP that develops endogenous islet amyloid deposits both *in vitro* and *in vivo* [10,32–35]. We performed *in vitro* studies to quantify islet amyloid deposition, islet cell death and caspase 3/7 activity in real-time using islets isolated from WT, Ripk3$^{-/-}$, hIAPP and hIAPP; Ripk3$^{-/-}$ mice. We evaluated hIAPP-stimulated inflammatory gene expression in WT and Ripk3$^{-/-}$ bone marrow derived macrophages (BMDM) *in vitro*, and we characterized the role of RIPK3 in glucose stimulated insulin secretion (GSIS) *in vitro* and *in vivo*. Lastly, we performed *in vivo* studies to examine body weight, glucose homeostasis, islet amyloid deposition and β-cell area in WT, Ripk3$^{-/-}$, hIAPP and hIAPP; Ripk3$^{-/-}$ mice in response to high fat diet (HFD) feeding. To our knowledge, this study is the first to evaluate the role of RIPK3 in HFD- and islet amyloid-induced β-cell cytotoxicity and hyperglycemia in a mouse model of T2D.

2. MATERIALS AND METHODS

2.1. Animals and islet isolations

Mice used in this study were maintained with ad libitum access to food and water under protocols approved by the Indiana University Institutional Animal Care and Use Committee. Mice carrying the hIAPP transgene were previously generated at the University of Washington [36]. Hemizygous hIAPP mice (hIAPP$^{+/0}$) that express hIAPP under control of the rat insulin II promoter and were maintained on a C57BL/6 x DBA/2J background. Whole body Ripk3 null mice on a C57BL/6 background (Ripk3$^{-/-}$, 025738, Jax, Bar Harbor, ME) and DBA/2J mice (000671, Jax) were obtained from Jackson Laboratories and backcrossed to obtain Ripk3$^{-/-}$ mice on a C57BL/6 x DBA/2J background. The Ripk3$^{-/-}$ mice used in these studies have an ENU-induced mutation in the donor splice site of intron 2 of the *Ripk3* gene that results in retention of intron 2 and introduction of an in-frame stop codon in the *Ripk3* RNA message. Ripk3$^{-/-}$ mice on a C57BL/6 x DBA/2J background were bred with hIAPP mice to obtain hIAPP; Ripk3$^{+/-}$ mice on a C57BL/6 x DBA/2J background. hIAPP; Ripk3$^{+/-}$ mice were then crossed with Ripk3$^{+/-}$ mice to generate hIAPP; Ripk3$^{-/-}$ mice and littermate controls for use in studies. At 8–10 weeks of age, male mice were fed a 45% kcal from fat high-fat diet (HFD) (D12451, Research Diets, New Brunswick, NJ) for the 12-month HFD study period. Islets were isolated from chow-fed 8- to 12-week-old male and female mice by the Indiana University Center of Diabetes and Metabolic Diseases Islet and Physiology Core (IU CDMD) or the University of Washington Diabetes Research Center Cell Function and Analysis Core, then hand-picked and allowed to recover overnight prior to experimentation.

2.2. Cell line and islet culture

For *in vitro* endogenous islet amyloid formation experiments, islets were allowed to recover overnight in 11.1 mM glucose RPMI following isolation, transferred to 16.7 mM glucose RPMI prior to experimentation and evaluated for up to 96 h. INS-1 cells and mouse islets were cultured in RPMI 1640 media with 11.1 mM glucose, 10% fetal bovine serum (FBS), 1% sodium pyruvate and 1% penicillin-streptomycin. For islet macrophage depletion, islets were isolated from 8- to 12-week-old male and female mice, cultured in 11.1 mM glucose RPMI, then treated with either 1 mg/ml clodronate-containing liposomes (C-0010, Liposoma, Amsterdam, Netherlands) or 1 mg/ml PBS-containing liposomes (P-010, Liposoma) for 48 h. At the end of this culture period, islets were collected for RNA isolation. Bone marrow derived macrophages cells were cultured in MEM media (10-010, Corning), 10% FBS, 1% penicillin-streptomycin, 10 ng/ml M-CSF1 (416-ML, R&D Systems, Minneapolis, MN). Briefly, femur and tibia were isolated, washed in 70% ethanol, then placed in HBSS + 2% FBS (isolation buffer). Bone marrow was flushed into a petri dish containing isolation buffer, the cell suspension was filtered through a 40 μm cell strainer, and cells were counted. Media was changed on day 3 after plating and every 2 days thereafter. Cells obtained on day 7 were used as BMDMs, with BMDMs obtained from one mouse considered a single replicate. Cells and islets were maintained in a 37 °C incubator with 5% CO_2. The following reagents were applied to BMDM cultures: synthetic hIAPP (20 μM, AS-60254-1, Anaspec, Fremont, CA), synthetic rIAPP (20 μM, AS-60253-1, Anaspec).

2.3. Real-time islet amyloid formation, cell death, and caspase 3/7 activity assays

Islet amyloid formation and cell death were quantified in real time using a Sartorius Incucyte S3 live-cell imaging and analysis instrument (Sartorius, Göttingen, Germany). To quantify amyloid formation, single intact islets were added to each well of a 96-well round-bottom plate (7007, Corning, Corning, NY) containing 16.7 mM glucose and Thioflavin S (5 nM, T1892, MilliporeSigma, Burlington, MA). Amyloid deposition was quantified every 2 h for 96 h and reported as Thio S positive area normalized to islet brightfield area for each condition and replicate. To quantify cell death, single intact islets were added to each well of a 96-well round-bottom plate (7007, Corning) containing 16.7 mM glucose and Sytox green (100 nM, S7020, ThermoFisher Scientific, Waltham, MA). Cell death was quantified every 2 h for 96 h and reported as Sytox green positive area normalized to islet brightfield area for each condition and replicate. To quantify islet caspase 3/7 activity in real time, single intact islets were added to each well of a 96-well round-bottom plate (7007, Corning) containing 16.7 mM glucose and Incucyte Caspase 3/7 dye (5 μM, 4440, Sartorius). Caspase 3/7 activity was quantified every 2 h for 96 h and reported as caspase 3/7 positive area normalized to islet brightfield area for each condition and replicate. Alternatively, caspase 3/7 activity was quantified using a luminogenic caspase 3/7 substrate (G8090, Promega, Madison, WI). Briefly, following culture islets were lysed, caspase 3/7 substrate was added for 1 h, then luminescence was quantified using a microplate reader (BioTek Synergy H1, Agilent, Santa Clara, CA) and data were reported relative to control islets for each replicate.

2.4. Quantitative real-time reverse transcription polymerase chain reaction (qRT-PCR)

Total RNA was isolated from cells using the High Pure RNA Isolation Kit (11828665001, Roche, Basel, Switzerland), then reverse transcribed with the QuantiTect Reverse Transcription Kit (205311, Qiagen, Venlo, Netherlands) and cDNA was subjected to qRT-PCR. Data were normalized to *18S* rRNA levels and expressed as fold relative to control using the $2^{-\Delta\Delta Ct}$ method. Alternatively, data were normalized to *18S* rRNA or *Ppib* mRNA levels and expressed as ΔCT to the gene of

interest. All qRT-PCR data points represent means of triplicate technical determinations. The following Taqman probes (ThermoFisher Scientific) were used to quantify mRNA expression: *Ripk3* (Mm00444947_m1), *Emr1* (Mm00802529_m1), *Tnf* (Mm004432-58_m1), *Il1b* (Mm00434228_m1), *Nos2* (Mm00440502_m1), *Ppib* (Mm00478295_m1), and *18S rRNA (HS99999901_s1)*.

2.5. Immunoblot analysis

Islet cell lysates were prepared in lysis buffer containing 1% SDS, 0.1% NP-40, 0.2% sarkosyl, 10% glycerol, 1 mM dithiothreitol, 1 mM EDTA, 10 mM NaF, 50 mM Tris, and protease and phosphatase inhibitors (04693116001 and 0490683700; MilliporeSigma). BMDM cell lysates were prepared in lysis buffer containing 0.2% Triton X-100, 10 mM EDTA, 2 mM EGTA, 10 mM NaF, 50 mM Tris, and protease and phosphatase inhibitors (04693116001 and 0490683700; MilliporeSigma). Cell lysates were centrifuged at 10,000 $\times$ *g* for 10 min, supernatants collected, and protein concentrations determined by BCA assay (23227, ThermoFisher Scientific). Equal amounts of protein were separated on SDS-PAGE gels (4561093, BioRad, Hercules, CA) and transferred to PVDF membranes (IPVH00010, MilliporeSigma). Proteins were visualized using the following primary antibodies: RIPK3 (1:1000, ab62344, Abcam, Cambridge, UK), phospho-MLKL (1:500, ab196436, Abcam), β-ACTIN (1:2000, ab8226, Abcam). Primary antibodies were detected with goat anti-mouse 800 (1:5000, 926-32210, LI-COR) or donkey anti-rabbit 680 (1:5000, 926-68071, LI-COR) IRDye secondary antibodies (LI-COR, Lincoln, NE), and visualized with a LI-COR CLx imaging system. Representative immunoblot images are shown.

2.6. Blood glucose, intraperitoneal glucose tolerance and insulin tolerance tests

Prior to HFD feeding and every 4 weeks thereafter, non-fasting blood glucose was measured using a handheld glucometer (Contour Next, Bayer, Leverkusen, Germany). Fasting blood glucose measurements were collected after overnight fast using a handheld glucometer. Intraperitoneal glucose tolerance tests (IPGTTs) were performed following an overnight fast. Briefly, glucose was administered intraperitoneally at a dose of 2 g/kg body weight, then blood glucose was measured via tail vein at 0 (before glucose injection), 10, 20, 30, 60, 90 and 120 min after glucose injection using a handheld glucometer (Contour Next, Bayer). Intraperitoneal insulin tolerance tests (IPITTs) were performed following a 2 h fast. Briefly, insulin was administered intraperitoneally at a dose of 0.75 U/kg body weight, then blood glucose was measured at 0 (before insulin injection), 15, 30, 45, and 60 min after insulin injection using the handheld glucometer.

2.7. Insulin secretion assays

For *in vitro* GSIS, islets were isolated from 8- to 12-week-old male and female mice and cultured overnight in 11.1 mM glucose RPMI media. Briefly, 20 islets per condition were washed with Krebs—Ringer Bicarbonate HEPES buffer (KRBH: 134 mM NaCl, 4.8 mM KCl, 1 mM $CaCl_2$, 1.2 mM $MgSO_4$, 1.2 mM KH_2PO_4, 5 mM $NaHCO_3$, 10 mM HEPES, 0.1% BSA), preincubated in 2.8 mM glucose KRBH, then cultured in KRBH containing either 2.8 mM or 16.7 mM glucose for 1 h. For secreted insulin, supernatants were collected, centrifuged, transferred to fresh tubes and stored at −80 °C. For insulin content, islets were lysed, sonicated and stored at −80 °C. Secreted insulin was assayed with an insulin ultra-sensitive homogeneous time resolved fluorescence (HTRF) kit (62IN2PEG, Cisbio, Codolet, France) and insulin content was assayed with an insulin high range HTRF kit (62IN1PEG, Cisbio). For *in vivo* GSIS, mice were fasted overnight then intraperitoneal glucose was administered at a dose of 2 g/kg body weight. Blood samples were collected from the tail vein 0 (before glucose injection), 2 and 10 min after glucose injection, and serum was obtained. Serum insulin measurements were performed by the IU CDMD Translational Core using insulin ELISA assays (10-1247-01, Mercodia, Uppsala, Sweden).

2.8. Immunohistochemistry and quantitative microscopy

Pancreases were extracted and fixed in 10% neutral buffered formalin (SF100-4, ThermoFisher Scientific). Fixed pancreas samples were embedded in paraffin, processed, 4 μm sections were cut, then sections were stained as previously described [19]. Briefly, β cells were stained using mouse monoclonal anti-insulin antibody (I2018; MilliporeSigma) followed by goat anti-mouse Cy3 (115-165-146; Jackson ImmunoResearch, West Grove, PA). Amyloid fibrils were stained in Thioflavin S (5 mM) for 2 min followed by 10 dips in 70% ethanol and a 5 min wash in water at RT. Sections were then mounted with polyvinyl alcohol with 0.2% Hoechst and images were captured on a Zeiss LSM710 confocal microscope (Zeiss, Oberkochen, Germany). Islet area, β-cell area, and amyloid severity were quantified using a computer-based quantitative method described previously [4,32,37]. Briefly, areas of insulin and nuclei positivity consistent with islet morphology were identified and islet regions of interest were defined using Zen Blue 2.1 image analysis software (Zeiss). This software was then used to quantify islet areas as well as insulin-positive and amyloid-positive areas within islet regions of interest. Average islet area was quantified as (Σislet area)/number of islets quantified per mouse, β-cell area was quantified as (Σinsulin positive area)/(Σislet area) x 100% for each mouse and amyloid severity was quantified as (Σamyloid positive area)/(Σislet area) x 100% for each mouse. An average of 24 $\pm$ 4 islets were analyzed per mouse by an observer blinded to pancreas sample genotype [38]. Representative islet images are shown.

2.9. Statistical analyses

Two-tailed Student's t-tests were used to analyze data sets with two groups, and one-way analysis of variance (ANOVA) tests were used to analyze data sets with more than two groups. Significant ANOVA results were followed with Holm-Sidák post-tests to analyze differences between groups of interest. For islet amyloid deposition, non-parametric Mann—Whitney tests were used to analyze data sets with two groups, and non-parametric Kruskal—Wallis tests were used to analyze data sets with more than two groups. Significant Kruskal—Wallis tests were followed by Dunn's post-tests to analyze differences between groups of interest. Correlation analysis was performed by simple linear regression. Statistical tests were performed with GraphPad Prism 10 software (GraphPad, San Diego, CA). Data are presented as mean $\pm$ SEM. A value of $p < 0.05$ was considered significant.

3. RESULTS

3.1. Real time quantification of islet amyloid deposition, islet cell death and caspase 3/7 activity *in vitro*

We first quantified endogenous islet amyloid formation, islet cell death and caspase 3/7 activity in wild type mouse islets that express non-amyloidogenic rIAPP (WT) and hIAPP islets that express amyloidogenic hIAPP (hIAPP) during culture in 16.7 mM glucose media for 96 h. These experiments utilized a high-content live cell imaging and analysis platform that enables quantification of parameters of interest in real time in intact islets. Using Thioflavin S to visualize amyloid fibrils

[39], we found that amyloid deposits were present in hIAPP islets starting 24 h after culture in 16.7 mM glucose media (Figure 1A). Significant islet amyloid deposition was present in hIAPP islets after 48 h and 96 h of culture (Figure 1B—D), while as expected amyloid deposits were not observed in WT islets at any time during the 96 h culture period (Figure 1A—D). We next quantified islet cell death in real time using Sytox green, a membrane impermeable DNA binding dye [40]. We found that 16.7 mM glucose treatment increased cell death in both WT and hIAPP islets over the first 24 h (Figure 1E). However, islet cell death was significantly higher in amyloid-prone hIAPP islets compared to amyloid-free WT islets 48 h (Figure 1F) and 96 h (Figure 1G) post 16.7 mM glucose treatment, times at which amyloid formation was occurring in hIAPP but not WT islets (Figure 1E—H). Treatment with 16.7 mM glucose significantly increased caspase 3/7 activity in both WT and hIAPP islets over time (Figure 1I,J), with glucose-induced caspase 3/7 activation being higher in amyloid-forming hIAPP islets compared to WT islets after 48 h and 96 h of culture (Figure 1J). Notably, we observed that RIPK3 protein expression and MLKL phosphorylation were upregulated in amyloid-laden hIAPP islets compared to amyloid-free WT islets *in vitro*, indicating a role for RIPK3 in amyloid-induced islet cell death (Figure 1K—M). These data suggest that amyloid deposition leads to increased islet cell death that occurs in association with elevated caspase 3/7 and RIPK3 activity.

3.2. Loss of RIPK3 protects from amyloid-induced islet cell death *in vitro*

To investigate the role of RIPK3 in amyloid-induced islet cell death, we next evaluated islets isolated from WT, Ripk3$^{-/-}$, hIAPP and hIAPP; Ripk3$^{-/-}$ mice. Following 48 h and 96 h of culture in 16.7 mM glucose, both hIAPP and hIAPP; Ripk3$^{-/-}$ islets exhibited significant amyloid deposition, the quantity of which was not different between genotypes (Figure 2A—C). In contrast, we found that hIAPP; Ripk3$^{-/-}$ islets were protected from amyloid-induced cell death compared to hIAPP islets with intact RIPK3 expression after both 48 h and 96 h of culture (Figure 2D—F). Following culture in 16.7 mM glucose for 48 h, caspase 3/7 activity was increased both in amyloid-forming hIAPP islets and in hIAPP; Ripk3$^{-/-}$ islets compared to amyloid-free WT islets (Figure 2G). Similar to our previous experiments (Figure 1K,M), amyloid formation in hIAPP islets was associated with increased *Ripk3* mRNA expression, and we found that the amyloid-induced increase in *Ripk3* expression was abrogated in hIAPP; Ripk3$^{-/-}$ islets (Figure 2H). Figure 2I illustrates loss of RIPK3 protein expression in Ripk3$^{-/-}$ islets.

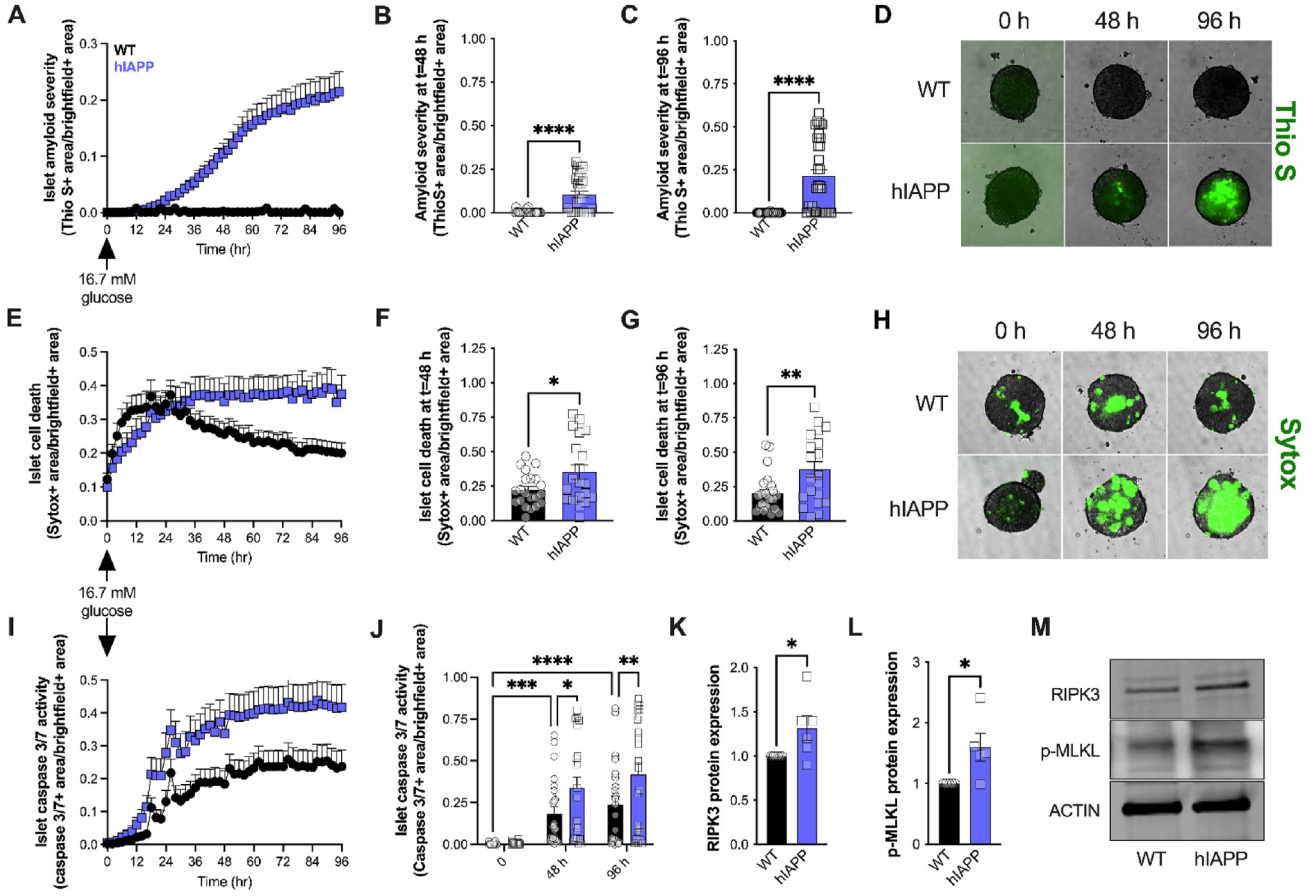

Figure 1: Real-time quantification of endogenous islet amyloid formation and islet cell death *in vitro*. Islet amyloid deposition, islet cell death and caspase 3/7 activity were quantified in intact islets isolated from WT (black, circles) and hIAPP (purple, squares) mice. **A)** Islet amyloid severity (Thio S + area/brightfield + area) was monitored every 2 h for 96 h and quantified at **B)** 48 h and **C)** 96 h post culture in 16.7 mM glucose (n = 34—35 islets from 4 mice per genotype). **D)** Representative images of islet amyloid deposition are shown. **E)** Islet cell death (Sytox + area/brightfield + area) was monitored every 2 h for 96 h and quantified at **F)** 48 h and **G)** 96 h post culture in 16.7 mM glucose (n = 20—23 islets from 3 mice per genotype). **H)** Representative images of islet cell death are shown. **I)** Islet caspase 3/7 activity (caspase 3/7+ area/brightfield + area) was monitored every 2 h for 96 h and quantified at **J)** 0, 48 and 96 h post culture in 16.7 mM glucose (n = 23—24 islets from 3 mice per genotype). **K)** RIPK3 and **L)** phospho-MLKL protein expression were quantified in WT and hIAPP islets following culture in 16.7 mM glucose (n = 5—6 per genotype). **M)** Representative images of RIPK3, phospho-MLKL and ACTIN protein expression are shown. *p < 0.05; **p < 0.01; ***p < 0.001; ****p < 0.0001.

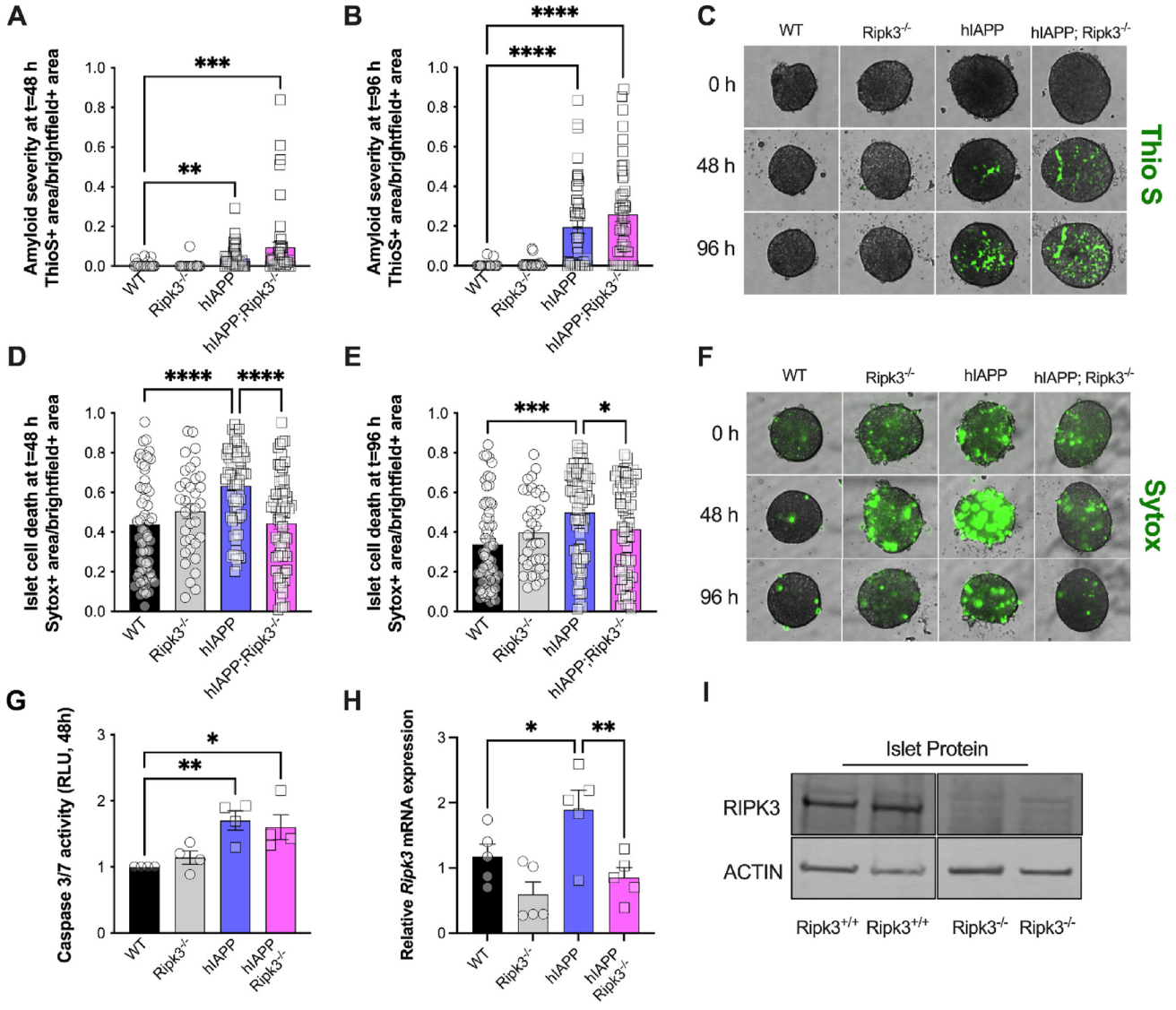

Figure 2: Loss of RIPK3 protects from amyloid-induced islet cell death *in vitro*. Islet amyloid deposition, islet cell death and caspase 3/7 activity were quantified in intact islets isolated from WT (black, circles), Ripk3$^{-/-}$ (gray, circles), hIAPP (purple, squares) and hIAPP; Ripk3$^{-/-}$ (pink, squares) mice. Islet amyloid severity (Thio S+ area/brightfield + area) was quantified at **A)** 48 h and **B)** 96 h post culture in 16.7 mM glucose (n = 24–48 islets from 3 to 6 mice per genotype). **C)** Representative images of islet amyloid deposition are shown. Islet cell death (Sytox + area/brightfield + area) was quantified at **D)** 48 h and **E)** 96 h post culture in 16.7 mM glucose (n = 36–72 islets from 4 to 8 mice per genotype). **F)** Representative images of islet cell death are shown. **G)** Caspase 3/7 activity was quantified in WT, Ripk3$^{-/-}$, hIAPP and hIAPP; Ripk3$^{-/-}$ islets 48 h post culture in 16.7 mM glucose and expressed relative to WT islets (n = 4 per genotype). **H)** *Ripk3* RNA expression was quantified in WT, Ripk3$^{-/-}$, hIAPP and hIAPP; Ripk3$^{-/-}$ islets following culture in 16.7 mM glucose for 48 h (n = 5 per genotype). **I)** RIPK3 protein expression was quantified in WT and Ripk3$^{-/-}$ mouse islets. Representative images of RIPK3 and ACTIN protein expression from non-consecutive lanes on the same membrane are shown. *p < 0.05; **p < 0.01; ***p < 0.001; ****p < 0.0001.

These results indicate that RIPK3 promotes amyloid-induced islet cell death downstream of amyloid deposition *per se*.

3.3. RIPK3 promotes hIAPP-induced inflammatory gene expression in macrophages *in vitro*

We next examined the role of RIPK3 in hIAPP-induced inflammatory gene expression *in vitro*. We first compared *Ripk3* expression in isolated islets, BMDMs and INS-1 β cells, and consistent with previous reports we found that *Ripk3* is expressed in each of these cell types (Figure 3A). We also observed that isolated islets express the macrophage marker *Emr1* (Figure 3B), suggesting that a portion of islet *Ripk3* expression may come from macrophages. To characterize the contribution of islet *Ripk3* expression from β cells versus macrophages more directly, we treated isolated islets with clodronate liposomes to deplete macrophages (Figure 3C–E). We found that clodronate-liposome treatment reduced islet *Emr1* expression by ~75% compared to islets treated with PBS liposomes (Figure 3D), indicating efficient clodronate-mediated macrophage depletion in this model. Islet *Ripk3* expression was also significantly reduced following clodronate-liposome treatment (Figure 3C), and the degree of *Ripk3* expression was correlated with the degree of *Emr1* expression in both PBS-liposome and clodronate-liposome treated islets (Figure 3E). These data indicate that in addition to β cells, macrophages are an important source of *Ripk3* expression in isolated islets. We next exposed WT and Ripk3$^{-/-}$ BMDMs to non-amyloidogenic synthetic rIAPP or amyloidogenic synthetic hIAPP for 16 h. Synthetic hIAPP, but

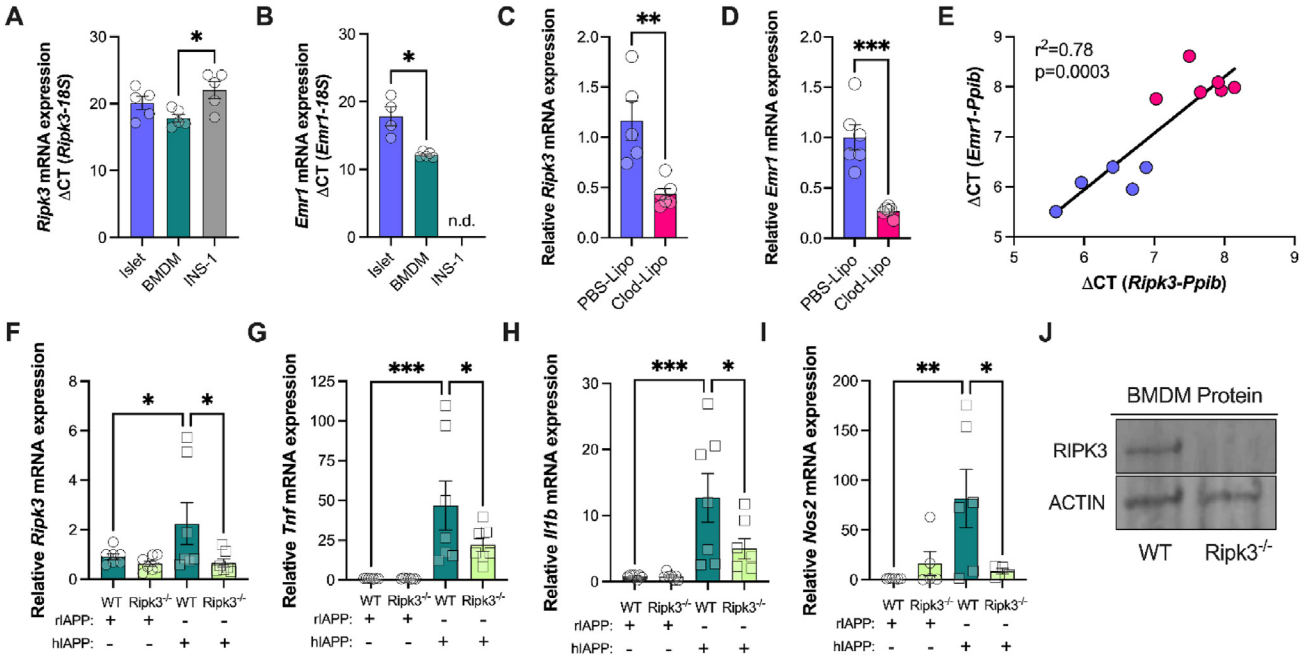

Figure 3: RIPK3 promotes synthetic hIAPP-induced inflammatory gene expression in macrophages *in vitro*. **A)** *Ripk3* and **B)** *Emr1* RNA expression was quantified in mouse islets (purple), bone marrow derived macrophage (BMDMs) (dark green) and INS-1 β cells (gray) and expressed as ΔCT to *18S* rRNA (n = 4–5 per cell type). Isolated mouse islets were cultured with PBS- (purple) or clodronate-containing liposomes (red) for 48 h. Expression of **C)** *Ripk3* and **D)** *Emr1* RNA was quantified and expressed relative to *Ppib* RNA levels using the $2^{-\Delta\Delta Ct}$ method (n = 5–6 per condition). **E)** Simple regression analysis of ΔCT values of *Emr1* (*Emr1 - Ppib* RNA) and *Ripk3* (*Ripk3 - Ppib* RNA) within PBS-liposome (purple) and clodronate-liposome (red) treated islets was performed. BMDMs isolated from WT mice (dark green) or Ripk3$^{-/-}$ mice (light green) were treated with synthetic rodent IAPP (circles) or synthetic human IAPP (squares) for 16 h. Expression of **F)** *Ripk3,* **G)** *Tnf,* **H)** *Il1b* and **I)** *Nos2* RNA was quantified and normalized to *18S* rRNA levels using the $2^{-\Delta\Delta Ct}$ method (n = 7 per condition). **J)** RIPK3 protein expression was evaluated in WT and Ripk3$^{-/-}$ BMDMs and representative immunoblots are shown. *p < 0.05; **p < 0.01; ***p < 0.001.

not rIAPP, significantly increased *Ripk3* expression in WT BMDMs, and this effect was blocked in Ripk3$^{-/-}$ BMDMs (Figure 3F). In addition, we found that synthetic hIAPP increased *Tnf* (Figure 3G), *Il1b* (Figure 3H) and *Nos2* (Figure 3I) expression in WT BMDMs, and these effects were ameliorated in Ripk3$^{-/-}$ BMDMs (Figure 3J). Together, these data indicate that loss of RIPK3 in macrophages mitigates islet amyloid-induced inflammation.

3.4. Characterization of metabolic phenotypes in chow-fed WT, Ripk3$^{-/-}$, hIAPP and hIAPP; Ripk3$^{-/-}$ mice

To evaluate the role of RIPK3 in metabolic phenotypes *in vivo*, we first examined chow-fed 8- to 12- week-old WT, Ripk3$^{-/-}$, hIAPP and hIAPP; Ripk3$^{-/-}$ mice. Mice from all groups exhibited similar glucose tolerance (Figure 4A,B), fasting blood glucose (Figure 4C), insulin tolerance (Figure 4D,E) and fasting serum insulin (Figure 4F) at this time. Following *in vivo* intraperitoneal glucose challenge, WT, Ripk3$^{-/-}$, hIAPP and hIAPP; Ripk3$^{-/-}$ mice exhibited similar insulin release 2 min and 10 min post glucose injection (Figure 4G). Moreover, *in vitro* GSIS (Figure 4H) and insulin content (Figure 4I) were similar between islets isolated from WT and Ripk3$^{-/-}$ mice. These data indicate that glucose homeostasis and β-cell secretory function are similar between young chow-fed WT, Ripk3$^{-/-}$, hIAPP and hIAPP; Ripk3$^{-/-}$ mice.

3.5. Loss of RIPK3 protects against and islet amyloid-induced glucose intolerance following HFD *in vivo*

We next evaluated the role of RIPK3 in HFD- and islet amyloid-induced glucose homeostasis *in vivo*. We quantified body weight, non-fasting blood glucose, glucose tolerance and insulin tolerance in WT, Ripk3$^{-/-}$, hIAPP and hIAPP; Ripk3$^{-/-}$ mice during and after 52 weeks of HFD feeding. All groups of mice gained body weight over the HFD feeding period (Figure 5A), and after 52 weeks of HFD hIAPP; Ripk3$^{-/-}$ mice exhibited higher body weight than WT, Ripk3$^{-/-}$ or hIAPP mice (Figure 5B). Non-fasting blood glucose concentrations were not different between groups over the course of the 52-week HFD feeding period (Figure 5C), and at study end non-fasting blood glucose (Figure 5D) and non-fasting serum insulin (Figure 5E) were not different between groups. In contrast, we found that islet amyloid-prone hIAPP mice exhibited significant glucose intolerance compared to WT mice after 52 weeks of HFD feeding, whereas hIAPP; Ripk3$^{-/-}$ mice were protected from amyloid-associated glucose intolerance (Figure 5F,G). Despite the higher body weight in hIAPP; Ripk3$^{-/-}$ mice at study end, insulin tolerance was not different among groups after HFD (Figure 5H,I). These data indicate that RIPK3 contributes to islet amyloid-induced glucose intolerance *in vivo*.

3.6. RIPK3 deficient mice are protected from islet amyloid-induced β-cell loss *in vivo*

To determine whether RIPK3 contributes to islet amyloid-induced β-cell loss *in vivo*, we next performed immunohistochemistry and quantitative microscopy on pancreas sections isolated from WT, Ripk3$^{-/-}$, hIAPP and hIAPP; Ripk3$^{-/-}$ mice following 52 weeks of HFD feeding. We found that average islet area was not different between WT, Ripk3$^{-/-}$, hIAPP and hIAPP; Ripk3$^{-/-}$ mice (Figure 6A). As expected, islet amyloid deposition was absent in pancreases from WT and Ripk3$^{-/-}$ mice that express rIAPP (Figure 6B). In contrast, significant islet amyloid deposition was observed in both hIAPP and hIAPP; Ripk3$^{-/-}$ pancreas sections, and the degree of islet amyloid deposition was not different between these genotypes (Figure 6B). Additionally,

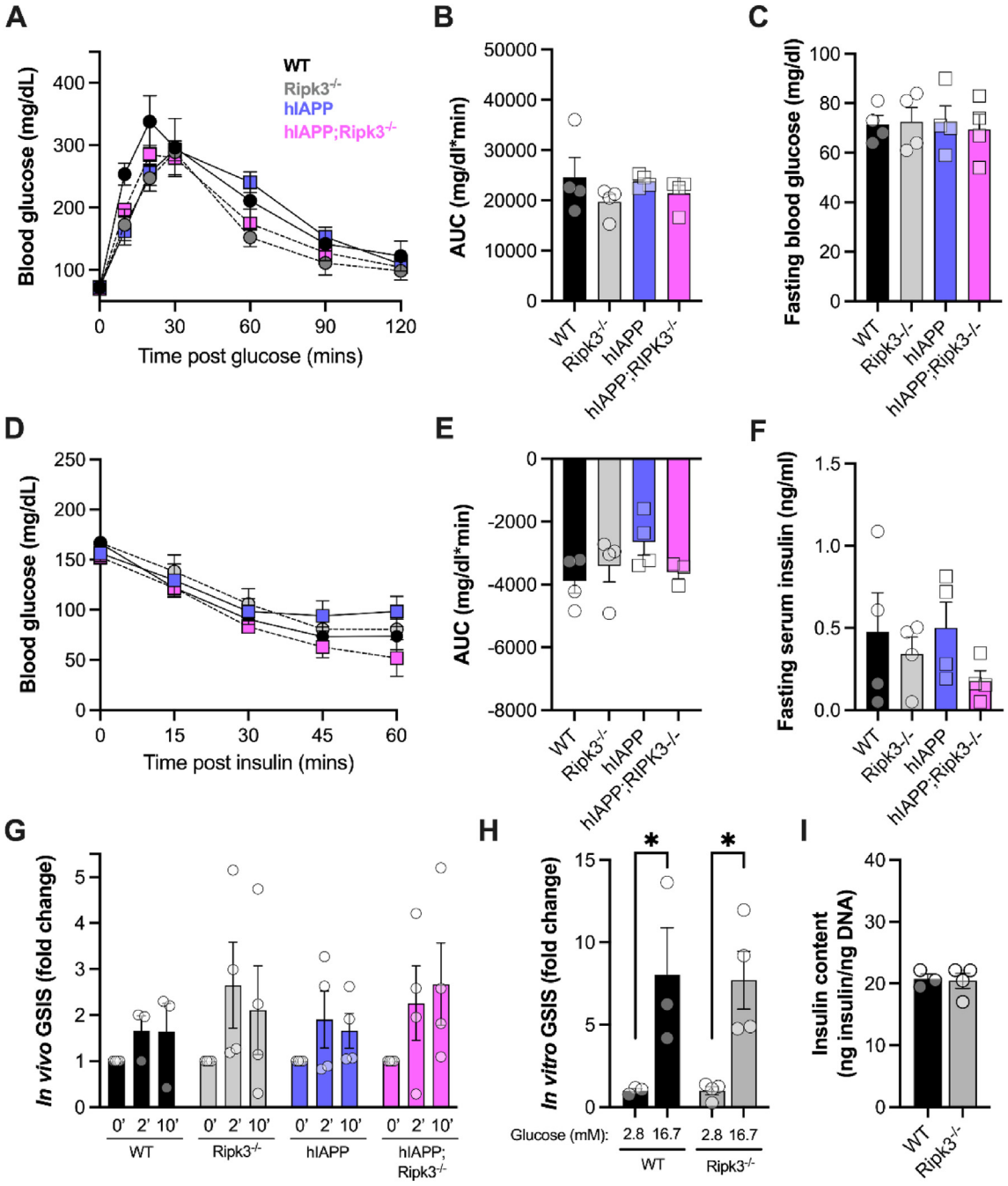

Figure 4: Characterization of metabolic phenotypes in chow-fed WT, Ripk3$^{-/-}$, hIAPP and hIAPP;Ripk3$^{-/-}$ mice. 8- to 12-week-old WT (black, circles), Ripk3$^{-/-}$ (gray, circles), hIAPP (purple, squares) and hIAPP; Ripk3$^{-/-}$ (pink, squares) mice fed a normal chow diet were examined. **A)** Glucose tolerance was evaluated by intraperitoneal glucose tolerance test (IPGTT) and **B)** quantified as incremental area under the curve (iAUC, mg/dl min) after overnight fast (n = 4 mice per genotype). **C)** Fasting blood glucose was measured by handheld glucometer after overnight fast (n = 4 mice per genotype). **D)** Insulin tolerance was evaluated by intraperitoneal insulin tolerance test (IPITT) and **E)** quantified as decremental area under the curve (dAUC, mg/dl min) after 2 h fast (n = 3–4 mice per genotype). **F)** Fasting serum insulin was measured after overnight fast (n = 4 mice per genotype). **G)** *In vivo* glucose stimulated insulin secretion (GSIS) was performed and serum insulin levels quantified at 0, 2 and 10 min following glucose challenge (n = 3–4 mice per genotype). *In vitro* GSIS was performed on islets isolated from 8 to 12-week-old WT and Ripk3$^{-/-}$ mice, then **H)** insulin secretion (fold change) and **I)** insulin content was measured (n = 3–4 mice per genotype). *p < 0.05.

we found that β-cell area was significantly reduced in amyloid-laden hIAPP versus amyloid-free WT pancreas sections (63.8 ± 3.1% versus 73.7 ± 0.7% β-cell area), and that hIAPP; Ripk3$^{-/-}$ pancreases were partially protected from this amyloid-induced β-cell loss (69.5% ± 1.8% β-cell area) (Figure 6C). Representative images of islets are shown in Figure 6D. These data suggest that loss of RIPK3 protects from amyloid-induced β-cell loss *in vivo* via mechanisms downstream of amyloid deposition *per se*.

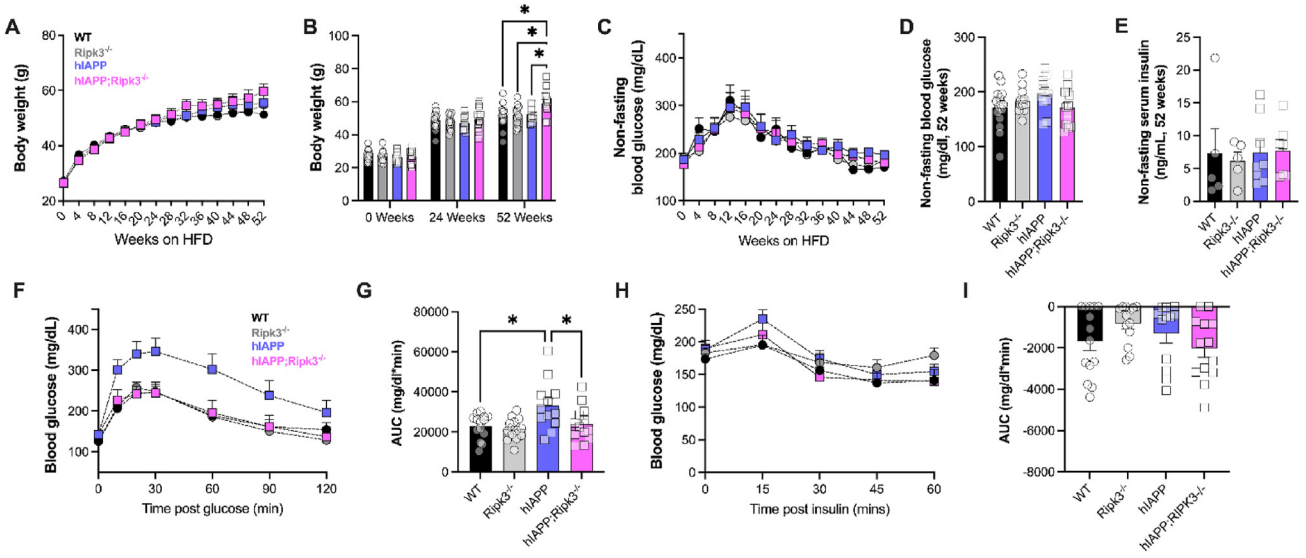

Figure 5: Loss of RIPK3 protects against amyloid-induced glucose intolerance *in vivo*. 8- to 10-week-old WT (black, circles), Ripk3$^{-/-}$ (gray, circles), hIAPP (purple, squares) and hIAPP; Ripk3$^{-/-}$ (pink, squares) mice were subjected to high-fat diet (HFD) feeding for 52 weeks. **A)** Body weight was monitored every 4 weeks for 52 weeks and **B)** quantified after 0, 24 and 52 weeks of HFD (n = 12–14 mice per genotype). **C)** Non-fasting blood glucose was monitored every 4 weeks for 52 weeks and **D)** quantified after 52 weeks of HFD (n = 12–14 mice per genotype). **E)** Non-fasting serum insulin was measured after 52 weeks of HFD feeding. **F)** Glucose tolerance was evaluated by intraperitoneal glucose tolerance test (IPGTT) and **G)** quantified as incremental area under the curve (iAUC, mg/dl min) after overnight fast (n = 12–14 mice per genotype). **H)** Insulin tolerance was evaluated by intraperitoneal insulin tolerance test (IPITT) and **I)** quantified as decremental area under the curve (dAUC, mg/dl min) after 2 h fast (n = 12–14 mice per genotype). *p < 0.05.

4. DISCUSSION

Islet amyloid deposition was first identified as a pathological feature of diabetes in 1901 [41], and numerous studies since then have established islet amyloid as a hallmark of the islet lesion in T2D [4,6,10,11,42]. Although islet amyloid is known to contribute to reduced β-cell mass, insufficient insulin secretion and hyperglycemia in T2D [3,4,10,32,35], the mechanisms that underlie this process remain incompletely understood. Here, we generated and evaluated islet amyloid-prone hIAPP mice with whole body loss of RIPK3, a recently recognized regulator of β-cell fate [25,26]. Our *in vitro* studies quantified amyloid deposition and cell death in intact isolated islets in real time,

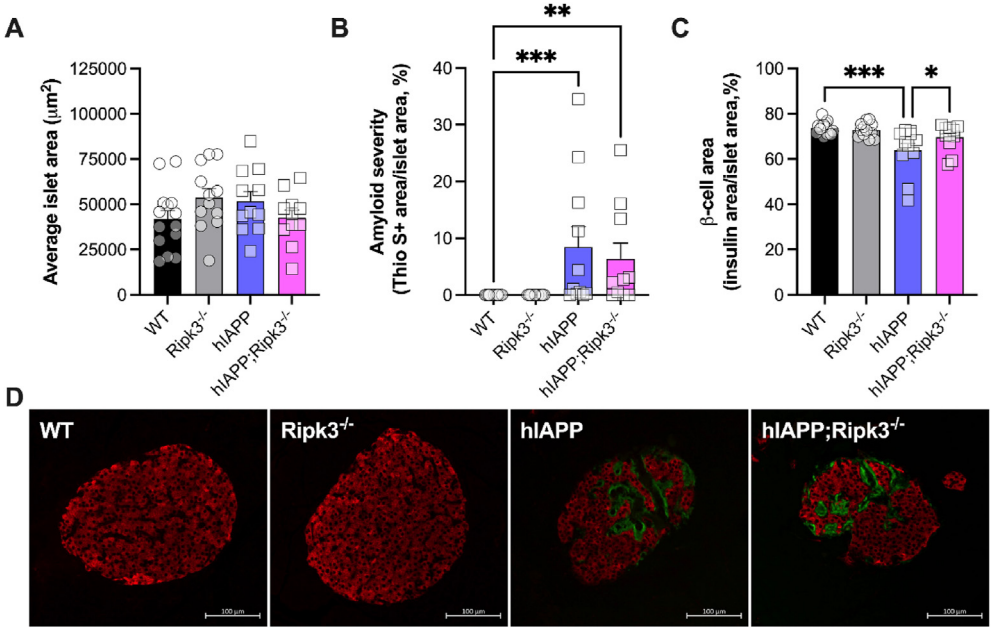

Figure 6: Loss of RIPK3 ameliorates amyloid-induced β-cell loss *in vivo*. After 52 weeks of HFD feeding, immunohistochemistry was performed on WT (black, circles), Ripk3$^{-/-}$ (gray, circles), hIAPP (purple, squares) and hIAPP; Ripk3$^{-/-}$ (pink, squares) mouse pancreas sections. **A)** Average islet area (μm^2), **B)** amyloid severity (Thio S+ area/islet area, %) and **C)** β-cell area (insulin + area/islet area, %) were quantified (n = 11–14 genotype). **D)** Representative images of pancreatic islets from WT, Ripk3$^{-/-}$, hIAPP and hIAPP; Ripk3$^{-/-}$ mouse pancreas sections are shown. Scale bar = 100 μm *p < 0.05; **p < 0.01; ***p < 0.001.

examined amyloid-induced caspase activation, and evaluated hIAPP-stimulated inflammatory gene expression. In addition, we performed *in vivo* studies on mice fed a HFD for 52 weeks to characterize the role of RIPK3 in islet amyloid deposition, amyloid-induced β-cell loss and hyperglycemia *in vivo*. Using this approach, we found that RIPK3 contributes to islet amyloid-induced inflammation, β-cell loss and glucose intolerance in a humanized mouse model of T2D.

In the present study, we evaluated potential roles of RIPK3 in amyloid-induced β-cell cytotoxicity. As described, our findings suggest that loss of RIPK3 protects from amyloid-induced islet cell death downstream of amyloid formation *per se*, likely via reduced amyloid-associated islet inflammation and β-cell death signaling. Given that RIPK3 can promote both caspase-mediated apoptosis [29,30] and caspase-independent necroptosis [23,31], we examined the roles of caspase 3/7 activity and RIPK3 expression in amyloid-induced β-cell loss *in vitro*. Similar to previous reports [43,44], we found that caspase activity was increased over time in association with islet amyloid deposition and islet cell death. However, our studies also found that protection from amyloid-induced cell death in hIAPP; Ripk3$^{-/-}$ islets was not coincident with reduced caspase 3/7 activity, and although hIAPP; Ripk3$^{-/-}$ islets were protected from amyloid-induced cell death, it was not blocked completely. Considering that we also observed increased RIPK3 expression and MLKL phosphorylation in amyloid-laden islets, our data indicate that both caspase-dependent mechanisms such as apoptosis and caspase-independent mechanisms such as necroptosis may contribute to amyloid-induced islet cell death *in vitro*. In this context, our findings are in agreement with a previous study showing that loss of caspase 8 in β cells reduces, but does not completely prevent, amyloid-induced β-cell death [43]. We propose a model wherein amyloid formation activates RIPK3 in coordination with caspase 8, and that RIPK3 promotes amyloid-induced islet cell death via caspase 3/7 independent actions. This model is in line with studies in other cell types that show caspase 8 and RIPK3 coordinately regulate caspase-dependent apoptosis and caspase-independent necroptosis signaling [22,24,45]. Our findings are also in agreement with recent observations of RIPK3 in AD pathogenesis [20,46] and suggest potential overlapping mechanisms of amyloid-associated cytotoxicity in AD and T2D.

In addition to its role in apoptotic and necroptotic cell death signaling, RIPK3 also regulates cytokine and chemokine production in immune cells [28,47,48]. Since islet amyloid deposition elicits cytokine production from islet resident macrophages [5,17] and synthetic hIAPP treatment increases inflammatory gene expression in macrophages and dendritic cells [17,49], we reasoned that the protection from amyloid-induced cell death observed in hIAPP; Ripk3$^{-/-}$ islets could be related to effects on RIPK3-mediated inflammation [47,48,50]. Indeed, we found that clodronate liposome-mediated depletion of islet macrophages reduced *Ripk3* expression *in vitro*, confirming that macrophages are an important source of islet *Ripk3* expression. In line with previous findings [17,49], we observed that synthetic hIAPP treatment increased *Tnf*, *Il1b* and *Nos2* gene expression in WT BMDMs, and this was associated with increased *Ripk3* expression. In contrast, we found that Ripk3$^{-/-}$ BMDMs were protected from synthetic hIAPP-induced inflammatory gene expression. Although RIPK3 has previously been shown to promote TNFα, IL1β and iNOS synthesis [24,27,47,51], our findings reveal this is also the case with hIAPP-stimulated inflammatory gene expression. Given these findings, we propose that macrophage RIPK3 promotes amyloid-induced islet inflammation separately from the known roles of RIPK3 in β cells [25,26]. As such, additional studies are needed to determine the relative importance of RIPK3 signaling in β cells versus macrophages in islet amyloid-induced β-cell cytotoxicity.

To explore the role of RIPK3 in T2D pathogenesis, we evaluated amyloid-free WT and Ripk3$^{-/-}$ mice as well as islet amyloid-prone hIAPP and hIAPP; Ripk3$^{-/-}$ mice *in vivo*. Prior to islet amyloid formation, we found that young, chow-fed WT, Ripk3$^{-/-}$, hIAPP and hIAPP; Ripk3$^{-/-}$ mice had similar glucose tolerance, fasting blood glucose, insulin tolerance and fasting serum insulin. These findings contrast with those of Roychowdhury et al. [52], and may be related to the different Ripk3 mutant mouse models used [53] and/or varying insulin secretory function between the different genetic backgrounds utilized in our studies [54]. Using our established HFD-feeding paradigm, we found that HFD led to islet amyloid deposition in both hIAPP and hIAPP; Ripk3$^{-/-}$ mice. While hIAPP mice exhibited glucose intolerance and reduced β-cell area following HFD, hIAPP; Ripk3$^{-/-}$ mice were protected from these impairments. The protection from glucose intolerance and β-cell loss observed in hIAPP; Ripk3$^{-/-}$ mice was not associated with improved insulin sensitivity or reduced islet amyloid deposition compared to hIAPP mice with intact RIPK3 expression, suggesting that loss of RIPK3 led to improved β-cell function and/or survival in the face of islet amyloid deposition. Moreover, since hIAPP and hIAPP; Ripk3$^{-/-}$ mice exhibited similar glucose tolerance and insulin sensitivity prior to HFD feeding, the glucose tolerance phenotypes observed were likely related to the HFD-induced islet amyloid deposition that occurred over the study period. Although β-cell function was not the focus of the present study, we observed that WT and Ripk3$^{-/-}$ islets had similar GSIS and insulin content *in vitro*, that young chow-fed WT, Ripk3$^{-/-}$, hIAPP and hIAPP; Ripk3$^{-/-}$ mice had similar GSIS *in vivo* and that WT, Ripk3$^{-/-}$, hIAPP and hIAPP; Ripk3$^{-/-}$ mice had similar non-fasting serum insulin following HFD feeding. However, we cannot rule out the possibility that higher insulin secretion in hIAPP; Ripk3$^{-/-}$ compared to hIAPP mice contributed to their improved glucose tolerance after HFD, as we did not quantify serum insulin in those particular studies. Given that RIPK3 is known to interact with molecules involved in amplification of insulin secretion such as glutamate dehydrogenase and isocitrate dehydrogenase 1 [55], studies of RIPK3 in the amplifying pathway of insulin secretion would be informative. However, like our *in vitro* studies, our *in vivo* data indicate that the protection observed in hIAPP; Ripk3$^{-/-}$ mice was not due to reduced amyloid deposition *per se*, but rather decreased amyloid-associated β-cell cytotoxicity.

Limitations to our studies exist. First, although we used a humanized mouse model of hIAPP expression that approximates amyloid deposition phenotypes in human islets, additional studies in *bona fide* human islets are needed to confirm the role of RIPK3 in amyloid-induced islet cytotoxicity in T2D. Given that we examined a mouse model of whole body RIPK3 deficiency, the phenotypes observed in hIAPP; Ripk3$^{-/-}$ islets and mice could be due to effects of RIPK3 in β cells, macrophages or other cell types. Our previous work revealed that RIPK3 regulates TNFα-induced cytotoxicity in β cells [26], and our current study identified a role for RIPK3 in hIAPP-stimulated inflammation in macrophages. Considering these findings, we believe RIPK3 could mediate amyloid-induced islet inflammation and β-cell death via actions in both cell types. However, additional studies using β-cell- or macrophage-specific models of RIPK3 deficiency are needed to determine whether loss of RIPK3 is beneficial due to reduced cell death signaling in β cells, decreased amyloid-induced cytokine production in macrophages, or both. Another caveat of our studies is that our quantification of cell death was performed using Sytox green, a membrane impermeable DNA-binding dye that labels both apoptotic and necroptotic cells [40]. Thus, our technique was not able to identify whether dead cells arising with amyloid deposition underwent apoptosis or necroptosis. Additionally, amyloid-induced cell death was

not quantified specifically in β cells but rather in all islet cell types. Although β cells comprise approximately 75% of mouse islets [56], it is possible that other islet cell types such as α cells, δ cells or macrophages were also captured in our *in vitro* cell death quantification. Future studies will characterize the protective phenotypes observed with RIPK3 deficiency in greater detail. Despite these limitations, the studies presented here identify RIPK3 as a novel mediator of islet amyloid-associated inflammation, β-cell loss and glucose intolerance.

4.1. Conclusions

In conclusion, our studies uncovered a novel role for RIPK3 in amyloid-associated β-cell loss and glucose intolerance in T2D pathogenesis. We found that loss of RIPK3 protects from amyloid-induced β-cell cytotoxicity and hIAPP-induced inflammation *in vitro* as well as amyloid-associated β-cell loss and glucose intolerance *in vivo*. This protection was not related to decreased amyloid deposition *per se*, indicating that RIPK3 mediates β-cell cytotoxicity downstream of amyloid formation via effects on amyloid-induced cytokine production and/or β-cell death signaling. Although RIPK3 has been identified as a potential therapeutic target in several diseases including cancer [57,58], acute kidney injury [59,60] and neurodegenerative diseases [20,22,46,61], this work shows that therapeutics targeting RIPK3 may also reduce β-cell cytotoxicity and promote glucose homeostasis during T2D pathogenesis.

FUNDING

This work was supported in part by funding from the U.S. Department of Veterans Affairs (IK2 BX004659 to ATT, I01 BX001060 to SEK), the National Institutes of Health (P30 DK097512 to Indiana University Center for Diabetes and Metabolic Diseases, P30 DK017047 to University of Washington Diabetes Research Center, T32 DK064466 to Indiana University Diabetes and Obesity Research Training Program), the Ralph W. and Grace M. Showalter Research Trust (080657-00002B to ATT), the VA Puget Sound Health Care System and the Richard L. Roudebush VA Medical Center.

CONTRIBUTION STATEMENT

N.M.: Conceptualization, formal analysis, investigation, methodology, writing — original draft, writing — review and editing; C.J.C., L.L., K.A.C., E.G.M., M.A.K. and N.E.: Investigation, methodology, writing — review and editing; S.E.K.: Conceptualization, methodology, funding acquisition, writing — review and editing; A.T.T.: Conceptualization, data curation, formal analysis, funding acquisition, investigation, methodology, supervision, writing — original draft, writing — review and editing.

ACKNOWLEDGMENTS

We thank Emily C. Sims and Matthew J. Repass (Indiana University School of Medicine Cellular Response Technologies Core) for expert assistance with Incucyte data collection and analysis. We thank Kara Orr and Lata Udari of the IU CDMD Islet and Physiology Core for expert assistance with islet isolation and metabolic phenotyping. We thank Mallory Oswalt, Anthony Acton Jr. and Robert V. Considine of the IU CDMD Translational Core for technical assistance with serum insulin measurements. We thank Alfred C. Aplin (Department of Veterans Affairs Puget Sound Health Care System, Seattle, WA) for technical assistance with gene expression analysis. Some data from this study were presented at the American Diabetes Association 83rd Scientific Sessions in 2023.

DECLARATION OF COMPETING INTEREST

All authors declare that no competing interests exist.

DATA AVAILABILITY

Data will be made available on request.

REFERENCES

[1] Kahn SE. The importance of beta-cell failure in the development and progression of type 2 diabetes. J Clin Endocrinol Metab 2001 Sep;86(9):4047—58.

[2] Cho NH, Shaw JE, Karuranga S, Huang Y, da Rocha Fernandes JD, Ohlrogge AW, et al. IDF Diabetes Atlas: global estimates of diabetes prevalence for 2017 and projections for 2045. Diabetes Res Clin Pract 2018 Apr 1;138:271—81.

[3] Kahn SE, Andrikopoulos S, Verchere CB. Islet amyloid: a long-recognized but underappreciated pathological feature of type 2 diabetes. Diabetes 1999 Feb 1;48(2):241—53.

[4] Jurgens CA, Toukatly MN, Fligner CL, Udayasankar J, Subramanian SL, Zraika S, et al. β-cell loss and β-cell apoptosis in human type 2 diabetes are related to islet amyloid deposition. Am J Pathol 2011 Jun 1;178(6):2632—40.

[5] Meier DT, Morcos M, Samarasekera T, Zraika S, Hull RL, Kahn SE. Islet amyloid formation is an important determinant for inducing islet inflammation in high-fat-fed human IAPP transgenic mice. Diabetologia 2014 Sep;57(9):1884—8.

[6] Butler AE, Janson J, Bonner-Weir S, Ritzel R, Rizza RA, Butler PC. Beta-cell deficit and increased beta-cell apoptosis in humans with type 2 diabetes. Diabetes 2003 Jan;52(1):102—10.

[7] Kahn SE, D'Alessio DA, Schwartz MW, Fujimoto WY, Ensinck JW, Taborsky Jr GJ, et al. Evidence of cosecretion of islet amyloid polypeptide and insulin by β-cells. Diabetes 1990 May 1;39(5):634—8.

[8] Westermark P, Engström U, Johnson KH, Westermark GT, Betsholtz C. Islet amyloid polypeptide: pinpointing amino acid residues linked to amyloid fibril formation. Proc Natl Acad Sci U S A 1990 Jul;87(13):5036—40.

[9] Lorenzo A, Razzaboni B, Weir GC, Yankner BA. Pancreatic islet cell toxicity of amylin associated with type-2 diabetes mellitus. Nature 1994 Apr;368(6473):756—60.

[10] Verchere CB, D'Alessio DA, Palmiter RD, Weir GC, Bonner-Weir S, Baskin DG, et al. Islet amyloid formation associated with hyperglycemia in transgenic mice with pancreatic beta cell expression of human islet amyloid polypeptide. Proc Natl Acad Sci U S A 1996 Apr 16;93(8):3492—6.

[11] Janson J, Soeller WC, Roche PC, Nelson RT, Torchia AJ, Kreutter DK, et al. Spontaneous diabetes mellitus in transgenic mice expressing human islet amyloid polypeptide. Proc Natl Acad Sci U S A 1996 Jul 9;93(14):7283—8.

[12] Lopes DHJ, Colin C, Degaki TL, Sousa ACV de, Vieira MNN, Sebollela A, et al. Amyloidogenicity and cytotoxicity of recombinant mature human islet amyloid polypeptide (hIAPP). J Biol Chem 2004 Oct 8;279(41):42803—10.

[13] Birol M, Kumar S, Rhoades E, Miranker AD. Conformational switching within dynamic oligomers underpins toxic gain-of-function by diabetes-associated amyloid. Nat Commun 2018 Apr 3;9(1):1312.

[14] Janson J, Ashley RH, Harrison D, McIntyre S, Butler PC. The mechanism of islet amyloid polypeptide toxicity is membrane disruption by intermediate-sized toxic amyloid particles. Diabetes 1999 Mar 1;48(3):491—8.

[15] Abedini A, Cao P, Plesner A, Zhang J, He M, Derk J, et al. RAGE binds pre-amyloid IAPP intermediates and mediates pancreatic β cell proteotoxicity. J Clin Investig 2018 Feb 1;128(2):682—98.

[16] Abedini A, Derk J, Schmidt AM. The receptor for advanced glycation end-products is a mediator of toxicity by IAPP and other proteotoxic aggregates: establishing and exploiting common ground for novel amyloidosis therapies. Protein Sci 2018 Jul;27(7):1166–80.
[17] Westwell-Roper CY, Ehses JA, Verchere CB. Resident macrophages mediate islet amyloid polypeptide-induced islet IL-1β production and β-cell dysfunction. Diabetes 2014 May;63(5):1698–711.
[18] Westwell-Roper CY, Chehroudi CA, Denroche HC, Courtade JA, Ehses JA, Verchere CB. IL-1 mediates amyloid-associated islet dysfunction and inflammation in human islet amyloid polypeptide transgenic mice. Diabetologia 2015 Mar;58(3):575–85.
[19] Templin AT, Mellati M, Meier DT, Esser N, Hogan MF, Castillo JJ, et al. Low concentration IL-1β promotes islet amyloid formation by increasing hIAPP release from humanised mouse islets in vitro. Diabetologia 2020 Nov;63(11):2385–95.
[20] Caccamo A, Branca C, Piras IS, Ferreira E, Huentelman MJ, Liang WS, et al. Necroptosis activation in Alzheimer's disease. Nat Neurosci 2017 Sep;20(9):1236–46.
[21] Zou C, Mifflin L, Hu Z, Zhang T, Shan B, Wang H, et al. Reduction of mNAT1/hNAT2 contributes to cerebral endothelial necroptosis and Aβ accumulation in Alzheimer's Disease. Cell Rep 2020 Dec 8;33(10):108447.
[22] Kumar S, Budhathoki S, Oliveira CB, Kahle AD, Calhan OY, Lukens JR, et al. Role of the caspase-8/RIPK3 axis in Alzheimer's disease pathogenesis and Aβ-induced NLRP3 inflammasome activation. JCI Insight 2023 Feb 8;8(3):e157433.
[23] Preston SP, Stutz MD, Allison CC, Nachbur U, Gouil Q, Tran BM, et al. Epigenetic silencing of RIPK3 in hepatocytes prevents MLKL-mediated necroptosis from contributing to liver pathologies. Gastroenterology 2022 Dec;163(6):1643–1657.e14.
[24] Moriwaki K, Bertin J, Gough PJ, Chan FKM. A RIPK3-Caspase 8 complex mediates atypical pro-IL-1β processing. J Immunol 2015 Feb 15;194(4):1938–44.
[25] Yang B, Maddison LA, Zaborska KE, Dai C, Yin L, Tang Z, et al. RIPK3-mediated inflammation is a conserved β cell response to ER stress. Sci Adv 2020;6(51):eabd7272.
[26] Contreras CJ, Mukherjee N, Branco RCS, Lin L, Hogan MF, Cai EP, et al. RIPK1 and RIPK3 regulate TNFα-induced β-cell death in concert with caspase activity. Mol Metab 2022 Nov 1;65:101582.
[27] Moriwaki K, Chan FKM. Necroptosis-independent signaling by the RIP kinases in inflammation. Cell Mol Life Sci 2016 Jun 1;73(11–12):2325–34.
[28] Orozco SL, Daniels BP, Yatim N, Messmer MN, Quarato G, Chen-Harris H, et al. RIPK3 activation leads to cytokine synthesis that continues after loss of cell membrane integrity. Cell Rep 2019 Aug 27;28(9):2275–2287.e5.
[29] Newton K, Dugger DL, Wickliffe KE, Kapoor N, Almagro MC de, Vucic D, et al. Activity of protein kinase RIPK3 determines whether cells die by necroptosis or apoptosis. Science 2014 Mar 21;343(6177):1357–60.
[30] Dondelinger Y, Aguileta MA, Goossens V, Dubuisson C, Grootjans S, Dejardin E, et al. RIPK3 contributes to TNFR1-mediated RIPK1 kinase-dependent apoptosis in conditions of cIAP1/2 depletion or TAK1 kinase inhibition. Cell Death Differ 2013 Oct;20(10):1381–92.
[31] Rodriguez DA, Weinlich R, Brown S, Guy C, Fitzgerald P, Dillon CP, et al. Characterization of RIPK3-mediated phosphorylation of the activation loop of MLKL during necroptosis. Cell Death Differ 2016 Jan;23(1):76–88.
[32] Hull RL, Andrikopoulos S, Verchere CB, Vidal J, Wang F, Cnop M, et al. Increased dietary fat promotes islet amyloid formation and beta-cell secretory dysfunction in a transgenic mouse model of islet amyloid. Diabetes 2003 Feb;52(2):372–9.
[33] Zraika S, Hull RL, Udayasankar J, Utzschneider KM, Tong J, Gerchman F, et al. Glucose- and time-dependence of islet amyloid formation in vitro. Biochem Biophys Res Commun 2007 Mar 2;354(1):234–9.
[34] Templin AT, Mellati M, Soininen R, Hogan MF, Esser N, Castillo JJ, et al. Loss of perlecan heparan sulfate glycosaminoglycans lowers body weight and decreases islet amyloid deposition in human islet amyloid polypeptide transgenic mice. Protein Eng Des Sel 2019 Dec 13;32(2):95–102.
[35] Templin AT, Meier DT, Willard JR, Wolden-Hanson T, Conway K, Lin YG, et al. Use of the PET ligand florbetapir for in vivo imaging of pancreatic islet amyloid deposits in hIAPP transgenic mice. Diabetologia 2018 Oct;61(10):2215–24.
[36] D'Alessio DA, Verchere CB, Kahn SE, Hoagland V, Baskin DG, Palmiter RD, et al. Pancreatic expression and secretion of human islet amyloid polypeptide in a transgenic mouse. Diabetes 1994 Dec;43(12):1457–61.
[37] Wang F, Hull RL, Vidal J, Cnop M, Kahn SE. Islet amyloid develops diffusely throughout the pancreas before becoming severe and replacing endocrine cells. Diabetes 2001 Nov 1;50(11):2514–20.
[38] Meier DT, Entrup L, Templin AT, Hogan MF, Samarasekera T, Zraika S, et al. Determination of optimal sample size for quantification of β-cell area, amyloid area and β-cell apoptosis in isolated islets. J Histochem Cytochem 2015 Aug;63(8):663–73.
[39] Bussière T, Bard F, Barbour R, Grajeda H, Guido T, Khan K, et al. Morphological characterization of Thioflavin-S-positive amyloid plaques in transgenic Alzheimer mice and effect of passive Aβ immunotherapy on their clearance. Am J Pathol 2004 Sep;165(3):987–95.
[40] Grootjans S, Hassannia B, Delrue I, Goossens V, Wiernicki B, Dondelinger Y, et al. A real-time fluorometric method for the simultaneous detection of cell death type and rate. Nat Protoc 2016 Aug;11(8):1444–54.
[41] Opie EL. The relation of diabetes mellitus to lesions of the pancreas. Hyaline degeneration of the islands of Langerhans. J Exp Med 1901 Mar 25;5(5):527–40.
[42] Maclean N, Ogilvie RF. Quantitative estimation of the pancreatic islet tissue in diabetic subjects. Diabetes 1955 Oct;4(5):367–76.
[43] Park YJ, Woo M, Kieffer TJ, Hakem R, Safikhan N, Yang F, et al. The role of caspase-8 in amyloid-induced beta cell death in human and mouse islets. Diabetologia 2014 Apr;57(4):765–75.
[44] Li H, Khosrow-Khavar F, Speck M, Kieffer T, Woo M, Marzban L. Suppression of caspase-3 activation protects primary islet β-cells from the cytotoxic effects of human islet amyloid polypeptide. Can J Diabetes 2008 Jan 1;32(4):302.
[45] Kaiser WJ, Upton JW, Long AB, Livingston-Rosanoff D, Daley LP, Hakem R, et al. RIP3 mediates the embryonic lethality of caspase-8-deficient mice. Nature 2011 Mar 17;471(7338):368–72.
[46] Abdelhady R, Younis NS, Ali O, Shehata S, Sayed RH, Nadeem RI. Cognitive enhancing effects of pazopanib in D-galactose/ovariectomized Alzheimer's rat model: insights into the role of RIPK1/RIPK3/MLKL necroptosis signaling pathway. Inflammopharmacology 2023 Oct 1;31(5):2719–29.
[47] Wong WWL, Vince JE, Lalaoui N, Lawlor KE, Chau D, Bankovacki A, et al. cIAPs and XIAP regulate myelopoiesis through cytokine production in an RIPK1- and RIPK3-dependent manner. Blood 2014 Apr 17;123(16):2562–72.
[48] Moriwaki K, Balaji S, McQuade T, Malhotra N, Kang J, Chan FKM. The necroptosis adaptor RIPK3 promotes injury-induced cytokine expression and tissue repair. Immunity 2014 Oct 16;41(4):567–78.
[49] Masters SL, Dunne A, Subramanian SL, Hull RL, Tannahill GM, Sharp FA, et al. Activation of the NLRP3 inflammasome by islet amyloid polypeptide provides a mechanism for enhanced IL-1β in type 2 diabetes. Nat Immunol 2010 Oct;11(10):897–904.
[50] Butcher MJ, Hallinger D, Garcia E, Machida Y, Chakrabarti S, Nadler J, et al. Association of proinflammatory cytokines and islet resident leucocytes with islet dysfunction in type 2 diabetes. Diabetologia 2014 Mar;57(3):491–501.
[51] Wu L, Zhang X, Zheng L, Zhao H, Yan G, Zhang Q, et al. RIPK3 orchestrates fatty acid metabolism in tumor-associated macrophages and hepatocarcinogenesis. Cancer Immunol Res 2020 May 1;8(5):710–21.
[52] Roychowdhury S, McCullough RL, Sanz-Garcia C, Saikia P, Alkhouri N, Matloob A, et al. Receptor interacting protein 3 protects mice from high-fat diet-induced liver injury. Hepatol 2016 Nov;64(5):1518–33.
[53] Newton K, Sun X, Dixit VM. Kinase RIP3 is dispensable for normal NF-kappa Bs, signaling by the B-cell and T-cell receptors, tumor necrosis factor receptor 1, and toll-like receptors 2 and 4. Mol Cell Biol 2004 Feb;24(4):1464–9.

[54] Andrikopoulos S, Massa CM, Aston-Mourney K, Funkat A, Fam BC, Hull RL, et al. Differential effect of inbred mouse strain (C57BL/6, DBA/2, 129T2) on insulin secretory function in response to a high fat diet. J Endocrinol 2005 Oct;187(1):45–53.

[55] Zhang DW, Shao J, Lin J, Zhang N, Lu BJ, Lin SC, et al. RIP3, an energy metabolism regulator that switches TNF-induced cell death from apoptosis to necrosis. Science 2009 Jul 17;325(5938):332–6.

[56] Cabrera O, Berman DM, Kenyon NS, Ricordi C, Berggren PO, Caicedo A. The unique cytoarchitecture of human pancreatic islets has implications for islet cell function. Proc Natl Acad Sci U S A 2006 Feb 14;103(7):2334–9.

[57] Liu S, Joshi K, Denning MF, Zhang J. RIPK3 signaling and its role in the pathogenesis of cancers. Cell Mol Life Sci 2021 Dec 1;78(23): 7199–217.

[58] Conev NV, Dimitrova EG, Bogdanova MK, Kashlov YK, Chaushev BG, Radanova MA, et al. RIPK3 expression as a potential predictive and prognostic marker in metastatic colon cancer. Clin Investig Med 2019 Mar 23;42(1):E31–8.

[59] Martin-Sanchez D, Guerrero-Mauvecin J, Fontecha-Barriuso M, Mendez-Barbero N, Saiz ML, Lopez-Diaz AM, et al. Bone marrow–derived RIPK3 mediates kidney inflammation in acute kidney injury. J Am Soc Nephrol 2022 Feb;33(2):357–73.

[60] Sureshbabu A, Patino E, Ma KC, Laursen K, Finkelsztein EJ, Akchurin O, et al. RIPK3 promotes sepsis-induced acute kidney injury via mitochondrial dysfunction. JCI Insight 2018;3(11):e98411.

[61] Oñate M, Catenaccio A, Salvadores N, Saquel C, Martinez A, Moreno-Gonzalez I, et al. The necroptosis machinery mediates axonal degeneration in a model of Parkinson disease. Cell Death Differ 2020 Apr;27(4):1169–85.

